Materials Science and Engineering C 57 (2015) 38–48

Contents lists available at ScienceDirect

Materials Science and Engineering C

journal homepage: www.elsevier.com/locate/msec

A highly efficient urea detection using flower-like zinc oxide nanostructures

Manvi Tak [a], Vinay Gupta [a], Monika Tomar [b,*]

[a] Department of Physics and Astrophysics, University of Delhi, Delhi 110007, India
[b] Department of Physics, Miranda House, University of Delhi, Delhi 110007, India

ARTICLE INFO

Article history:
Received 20 March 2015
Received in revised form 5 June 2015
Accepted 25 June 2015
Available online 11 July 2015

Keywords:
Urea
Zinc oxide
Flower-like nanostructures
Hydrothermal method
Biosensor

ABSTRACT

A novel matrix based on flower-like zinc oxide nanostructures (ZnONF) has been fabricated using hydrothermal method and exploited successfully for the development of urea biosensor. Urease (Urs) is physically immobilized onto the ZnO nanostructure matrix synthesized over platinized silicon substrate. The surface morphology and crystallographic structure of the as-grown ZnONF have been characterized using a scanning electron microscope (SEM) and X-ray diffraction (XRD) techniques. The fabricated amperometric biosensor (Urs/ZnONF/Pt/Ti/Si) exhibits a linear sensing response towards urea over the concentration range 1.65 mM to 16.50 mM with an enhanced sensitivity (~132 μA/mM/cm^2) and a fast response time of 4 s. The relatively low value of Michaelis–Menten constant (K_m) of 0.19 mM confirms the high affinity of the immobilized urease on the nanostructured ZnONF surface towards its analyte (urea). The obtained results demonstrate that flower-like ZnO nanostructures serve as a promising matrix for the realization of efficient amperometric urea biosensor with enhanced response characteristics.

1. Introduction

Recently, need for a continuous real time monitoring of toxic chemicals present in the environment known as pollutants has drastically increased. A lot of pollutants have been found at various stages during recycling and industrial processes; at agricultural, urban and industrial sites and in waste waters and effluents. Hence, for environmental monitoring, there is demand for techniques possessing fast-response, portability, high sensitivity, robustness and high shelf-life, which can be exhibited by the electrochemical methods for detection. There are several reports found in literature related to the environmental monitoring using electrochemical analysis, for e.g., Parvan et al. have reported results related to detection of hydroxylamine in water samples using electrochemical detection [1]. Not only in environmental but also in pharmaceuticals and health care industries as well as in clinical diagnosis field, electrochemical detection method has gained considerable attention. There are reports available in literature related to the detection of important drugs and chemicals for human body such as norepinephrine, N-acetylcysteine, epinephrine, isoproterenol and levodopa using electrochemical method [2–9]. This method has also been used for detecting a number of important biomolecules such as glucose, uric acid, cholesterol and urea present in the human body.

Urea is one of the important biomolecules present in the human body. It is produced in the human body from ammonia as a result of urea cycle or by oxidation of amino acids and is excreted out in urine. The optimum amount of urea in human blood/serum is 8–20 mg dL^{-1} and any discrepancy in its normal level may be dangerous [10]. Hence, its continuous monitoring is of utmost importance for the clinical purpose. The detection of urea is crucial not only in clinical diagnosis but also in other fields including agriculture and food science [10]. Thus, there has been a growing demand for the estimation of urea. Various methods are available for urea detection such as gas chromatography, calorimetry, fluorimetry, conductometry, inductometry and ion sensitive field effective transistors [11–15]. However, these techniques suffer from complicated sample pre-treatment steps and involve expensive instrumentation [11–15]. Electrochemical biosensors serve as an efficient alternative to overcome some of these problems. Few reports are available in literature aiming towards the development of the potentiometric urea biosensor with application of pH sensitive electrode or an ion selective electrode [16]. For instance, Ansari et al. have studied the effect of various ZnO nanostructures prepared by sol–gel technique on urea detection [17]. Though the reported biosensing results show wide detection range of urea but the sensitivity is very low and is not suitable for practical applications. Furthermore, the stability and interference related concerns have not been considered which are amongst the most essential characteristics required in assessing the performance of the biosensor [17]. Hence, limited success has been obtained on the fabrication of potentiometric urea biosensor, where poor selectivity as

* Corresponding author.
E-mail address: monikatomar@gmail.com (M. Tomar).

http://dx.doi.org/10.1016/j.msec.2015.06.052
0928-4931/

well as sensitivity has always been an issue of major concern. Alternatively, amperometric technique owing to its high sensitivity, selectivity and reproducibility eliminates such problems and so, has been the most preferred detection technique for various biomolecules [18].

A key parameter in fabrication of the amperometric biosensor is the identification of a suitable matrix which not only provides fast electron communication feature but also offers high surface area for high enzyme loading [19–24]. Amongst various matrices, nanostructured metal oxides are extensively exploited due to their unique properties including high surface to volume ratio, good stability, and favorable orientation for the immobilization of specific enzyme [24–28]. Recently, ZnO nanostructures have been utilized as an efficient matrix in the field of biosensing for detecting a number of biomolecules due to its good electron communication feature, wide band-gap, high chemical stability, good biocompatibility and most importantly high isoelectric point (IEP ~ 9.5) which is important for the immobilization of enzymes having low IEP such as urease (~4.0) by physical adsorption technique [21,29,30]. However, there have been very few reports in literature on the utilization of ZnO nanostructures for detecting urea using amperometric technique. For instance, there is a report by Ali et al. based on the fabrication of urea sensor using nanostructured zinc oxide film but the fabricated biosensor exhibits very low sensitivity (1.44 μA mM^{-1} cm^{-2}) as well as increased sensor cost due to utilization of double enzymes (i.e. urease and glutamate dehydrogenase) [31]. Another report by Palomera et al. is based on the fabrication of urea biosensor using ZnO nanorods which give a wide linear response for urea detection (i.e. 1–20 mM) and low detection limit (0.13 mM) but the sensitivity is very poor (0.40 μA mM^{-1} cm^{-2}) [32]. Hence, low sensitivity and stability are the main concerns which make these reported urea biosensors unsuitable for any practical commercial application thus giving a lot of scope for further improvement.

The sensitivity may be enhanced by improving the nanostructure morphology (different shapes) of the matrix for effective loading of the enzyme. On the other side the stability of biosensor depends on the quality of the matrix which in turn depends on its growth kinetics.

In order to improve these parameters, it is important to note that the grown nanostructures should be crystalline as high crystallinity results in larger grain size and reduced grain boundaries which promotes fast communication of the electrons and also provides better stability to the nanostructured bioelectrodes. Hydrothermal method is a well-known method for the synthesis of ZnO nanostructures of very high crystallinity as well as purity. Besides this, it is a comparatively easier, quicker and economical method for the nanostructure fabrication. Hence, looking at the advantages offered by the amperometric electrochemical detection technique and the hydrothermally route for nanostructure synthesis, an effort has been made in the present work to realize a simple electrochemical urea biosensor using ZnO nanostructures possessing flower-like morphology. Hence, the main emphasis is towards the development of hydrothermal assisted flower-like ZnO nanostructure matrix for effective loading of enzyme with fast electron communication features. Such matrix is expected to give enhanced response characteristics towards urea. To the best of our knowledge no report yet has been available in literature based on the electrochemical detection of urea utilizing presently fabricated unique nanostructure morphology bearing flower-like ZnO nanostructures.

2. Experimental

2.1. Materials

Urea, Urease (Urs) (Type (iii) from Jack Beans) procured from Sigma, USA. Zinc acetate dihydrate ($Zn(C_2H_3O_2)_2 \cdot 2H_2O$, 99.0%), Monoethanolamine (MEA) ($CH_2(OH)CH_2NH_2$, 99.0%), Methanol (CH_3OH, 99.0%), Zinc nitrate hexahydrate ($Zn(NO_3)_2 \cdot 6H_2O$, 99.0%) were purchased from Sigma-Aldrich, USA. Hexamine (HMTA) ($C_6H_{12}N_4$, 99.0%) was purchased from Titan Biotech Ltd., India. Sodium phosphate monobasic anhydrous and sodium phosphate dibasic dihydrate were obtained from Sisco Chemicals, India. All chemicals were used without further purification. 50 mM phosphate buffer saline (PBS), pH 7.0 (0.9% NaCl) solution was prepared by adjusting the proportion of monobasic sodium phosphate solution and dibasic sodium phosphate solution (Sisco Chemicals) and then adding 0.9% NaCl to the solution. Deionized (DI) water (resistivity ~ 18.2 MΩ-cm) was used for the preparation of aqueous solutions.

2.2. Synthesis of flower-like ZnO nanostructures

ZnO nanostructures have been synthesized by using a seeding layer of ZnO prepared by sol–gel followed by the hydrothermal growth process and is discussed in the following sections:

(i) Preparation of ZnO seeding layer: sol–gel method0.375 M zinc acetate solution was prepared in methanol at room temperature. MEA, a sol stabilizer, was added keeping 1:1 molar ratio of zinc acetate to MEA making the solution for seeding. The seed solution was stirred at 60 °C yielding a clear, transparent and homogeneous solution which was aged for 24 h. The solution, thus obtained, was spin coated onto Platinum (Pt) coated silicon substrate. A thin film of Pt (~100 nm) was coated on the Si substrate by RF sputtering technique using a metal Pt (99.99% pure) target in 100% Ar gas atmosphere at 10 mTorr sputtering pressure. A thin buffer layer of Ti (~20 nm) was sputter coated by sputtering prior to Pt deposition under the same deposition conditions to improve the adhesion of Pt on the Si substrate. Subsequently, the spin coated ZnO thin film was baked at 300 °C to remove residual solvents. The foregoing process of spin-coating and thereafter baking was repeated several times to obtain ZnO seeding layer of desired thickness.

(ii) Growth of flower-like ZnO nanostructures: hydrothermal processZnO nanostructures were synthesized on the seed layer using hydrothermal process at 90 °C for 4 h. For controlling the dimensions of the nanostructures, hydrothermal growth of ZnO nanostructures was carried out in various concentrations (0.005 M, 0.01 M and 0.02 M) of the zinc nitrate and HMTA equimolar aqueous solutions. The substrates were then removed from the solution followed by thorough washing with deionized water and then dried in air at room temperature.

2.3. Urea bioelectrode fabrication

20 μL of freshly prepared urease solution (1 mg/mL, in 50 mM PBS, pH 7.0) was immobilized onto the surface of ZnO nanostructure based electrode by physical adsorption and kept for 5–6 h for drying at room temperature. At the physiological pH of ~7.0, flower-like ZnO nanostructures having a relatively high isoelectric point (IEP ~ 9.5) behaves as a positively charged matrix which can have a strong interaction with molecules having low IEP like urase (IEP ~ 4.0) when immobilized on its surface. Urease is immobilized on the surface of ZnO nanostructured matrix by physical adsorption technique and a strong electrostatic interaction between them binds and the urease molecules on the surface of flower-like ZnO nanostructured matrix. Finally, the prepared bioelectrode was stored at 4 °C overnight followed by extensive washing with a PBS buffer to remove any unbound enzyme. The bioelectrode was stored at 4 °C when not in use. Different concentrations of urea solutions were prepared in DI water. The detailed schematic for the fabrication of the flower-like ZnO nanostructure based bioelectrode is shown in Scheme 1.

2.4. Biosensor characterizations and electrochemical measurements

The surface morphology and crystallographic structure of the prepared ZnONF matrix were characterized by scanning electron

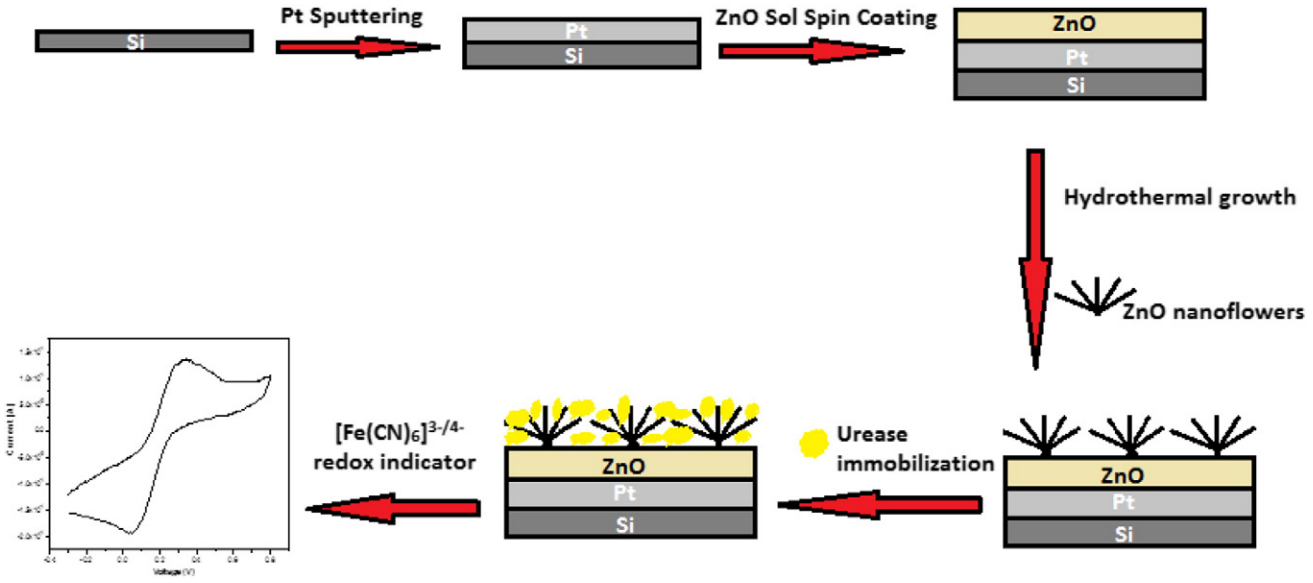

Scheme 1. Schematic of the fabrication of ZnONF bioelectrode for urea detection.

microscopy (SEM, Zeiss MA-15) and X-ray diffraction (XRD) studies (Bruker D8 Discover) respectively. The room temperature photoluminescence (PL) spectrum of the prepared ZnONF samples was measured to study the defect profile using spectroscopy with Horiba JobinYvon Lab Ram HR He-Cd laser ($\lambda = 325$ nm). Fourier transform infrared spectroscopy (FTIR) [Make: Perkin Elmer; model: Frontier] was employed to identify the phase purity of ZnO nanostructures (ZnONF) to confirm the immobilization of urease on the surface of developed matrix. The film thickness was measured using a surface profiler (Dektak 150A). Cyclic voltammetric (CV) measurements were

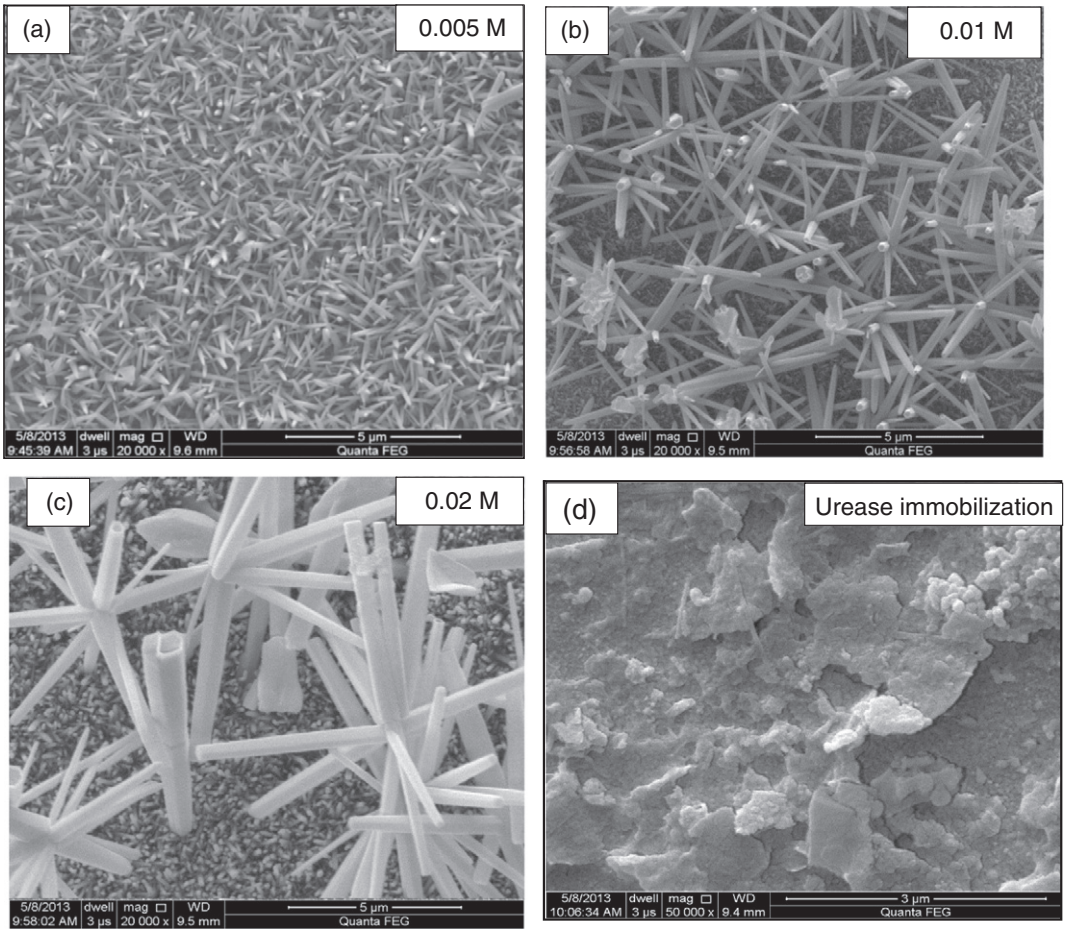

Fig. 1. SEM images of ZnONF/Pt/Ti/Si electrode prepared in (a) 0.005 M, (b) 0.01 M, (c) 0.02 M hydrothermal growth solution and (d) SEM image of urease immobilized on the surface of ZnONF/Pt/Ti/Si electrode (0.01 M).

carried out on a Potentiostat/Galvanostat (Gamry Inc. 600) using a three-electrode system in a PBS solution (50 mM, pH 7.0, 0.9% NaCl) containing 5 mM $[Fe(CN)6]^{3-/4-}$ as mediator with Ag/AgCl as the reference electrode. The photometric assay study was performed using a UV–visible spectrophotometer [Perkin Elmer Lamda 35].

3. Results and discussion

3.1. Structural and morphological studies

Fig. 1 shows the SEM images of the ZnO nanostructures obtained for different concentrations of growth solution (i.e. 0.005 M, 0.01 M and 0.02 M). It can be seen that the density as well as diameter of ZnO nanostructures increase upon increasing growth solution concentration. For 0.005 M concentrated growth solution (Fig. 1(a)), randomly oriented ZnO nanorods were observed and for 0.01 M (Fig. 1(b)), large flower-like morphologies were observed along with small nanorods. Large flower-like structures consist of radially oriented hexagonally shaped tip nanorods having ~2.5 μm and a diameter of ~160 nm. On further increasing molarity up to 0.02 M (Fig. 1(c)), the diameter increases to ~300 nm. After urease immobilization over the nanostructured sample surface (i.e. for 0.01 M), a thick deposited enzyme layer was observed (Fig. 1(d)) showing very high urease loading due to very high surface area provided by the grown ZnO nanostructures which results in complete coverage of the sample surface by the immobilized enzyme. The similar flower-like ZnO nanostructures were obtained for a number of samples prepared in different batches grown under identical conditions.

The suggested growth mechanism for the formation of flower-like ZnO nanostructures can be represented by the following reactions [34,35]:

$$C_6H_{12}N_4 + 6H_2O \rightarrow 6HCHO + 4NH_3 \quad (1)$$

$$NH_3 + H_2O \rightarrow NH_4^+ + OH^- \quad (2)$$

$$2OH^- + Zn^{2+} \rightarrow ZnO\,(s) + H_2O. \quad (3)$$

The ZnO nuclei gradually aggregate on various nucleating sites provided by the ZnO seeding layer and stack themselves in the shape of nanorods which further provide the nucleating centers for the building of ZnO flower-shaped morphologies. The driving force for the formation of nanostructures is the minimum surface energy or the growth velocity provided for nucleating centers on the substrate. Formation of ZnO nanorods only without flower-like morphologies for ~0.005 M concentrated growth solution (Fig. 1(a)) was found due to a comparatively lesser amount of Zn^{+2} and OH^- ions. It was observed that ZnO nanostructures can be grown for any concentrations, but the molarity of $Zn(NO_3)_2$ and HMTA must be equal.

The XRD spectra of the ZnONF onto Pt/Ti/Si substrate grown in various molarities (0.005 M, 0.01 M and 0.02 M) of the growth solution are shown in Fig. 2. All the samples show well defined peaks corresponding to either hexagonal structure of ZnO or the underneath Pt/Ti/Si substrate. The reflections corresponding to (100), (002) and (101) planes of ZnO are observed with preferred (002) orientation (Fig. 2), since, the growth velocity of ZnO structure is maximum towards (002), under hydrothermal conditions [36]. It is reported that the wurtzite structure of ZnO comprises of alternating planes composed of tetrahedrally coordinated Zn^{2+} and O^{2-} ions, stacked along c-axis [37]. The Zn^{2+} (001) is catalytically active while O^{2-} (001) is reported to be inert [37–39]. As the molarity of the growth solution increases from 0.005 M to 0.02 M (002) peak becomes more prominent which is due to increase in the concentration of Zn^{2+} and O^{2-} ions. The XRD analysis of the obtained data for various ZnONF samples grown in different concentrations (0.005 M, 0.01 M and 0.02 M) is shown in Table 1. It can be seen from Table 1 that with an increase in molarity from 0.005 M to 0.02 M, the 2θ value corresponding to (002) XRD peak shifts from higher to lower angle with respect to the ZnO bulk value. It can be observed from Table 1 that the crystallite size as well as stress increases from 24 nm to 32 nm with an increase in molarity of the growth solution. The sign of stress is found to be negative for the prepared ZnONF films in 0.005 M concentration and thereafter becomes positive because of the change in stress from compressive to tensile due to elongation of a unit cell along c-axis [40,41].

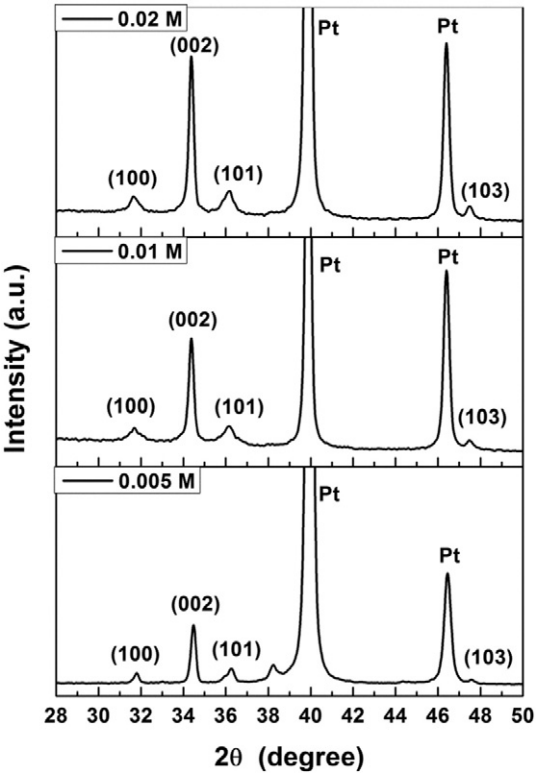

Fig. 2. XRD spectra for ZnONF films grown in 0.005 M, 0.01 M and 0.02 M concentrations of the growth solution.

3.2. Optical studies

Room temperature photoluminescence (PL) spectrum was recorded for the ZnONF sample hydrothermally grown in a 0.01 M solution (Fig. 3) using He–Cd laser (325 nm). An intense and sharp (UV) emission, at around 380 nm (Fig. 3) was observed due to the near band edge (NBE) emission corresponding to the recombination and emission of the free exciton through an exciton–exciton collision process [33] along with negligible visible region emission indicating that the as-grown ZnONF have a minimum amount of defects. The results confirm the formation of good quality highly crystalline ZnO nanostructures for fast electron communication.

The FTIR spectra of the ZnONF grown in a 0.01 M solution are shown in Fig. 4(a), exhibiting absorption bands at 422 cm^{-1} and 565 cm^{-1} which confirms the formation of ZnO. An intense FTIR band observed at 422 cm^{-1} reveals the formation of Zn–O bond and the band at 565 cm^{-1} is attributed to the stretching vibration of Zn–O [42,30].

Table 1
XRD analysis of theZnONF films grown in 0.005 M, 0.01 M and 0.02 M concentrations of the growth solution.

Molarity (M)	2θ (degree)	a = b (Å)	c (Å)	Crystallite size (nm)	Stress × 10^8 (N/m^2)
0.005	34.46	3.003	5.201	24.82	−4.75
0.01	34.37	3.010	5.214	27.14	6.66
0.02	34.369	3.010	5.216	32.16	6.79
ZnO bulk	34.42	3.249	5.206		

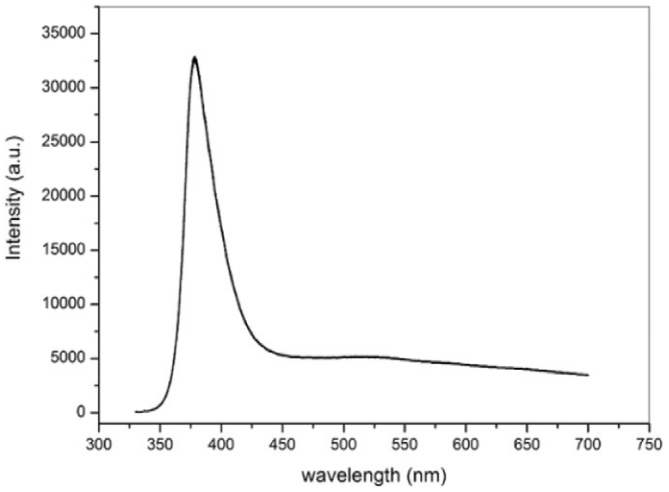

Fig. 3. Room temperature photoluminescence (PL) spectra of the ZnONF/Pt/Ti/Si electrode (0.01 M) using He–Cd laser (λ = 325 nm).

The absorption bands seen at around 3400 cm^{-1}, 1598 cm^{-1} and 1400 cm^{-1} correspond to O–H mode of vibration due to absorption of water molecules onto ZnONF surface [30,31]. Additional absorption bands at about 1542 cm^{-1}, 1652 cm^{-1} and 1003 cm^{-1} are observed in the FTIR spectra (Fig. 4(b)) of ZnONF after immobilization of urease enzyme on its surface and are due to amide bonds present in the protein, revealing immobilization of urease onto the surface of ZnONF via

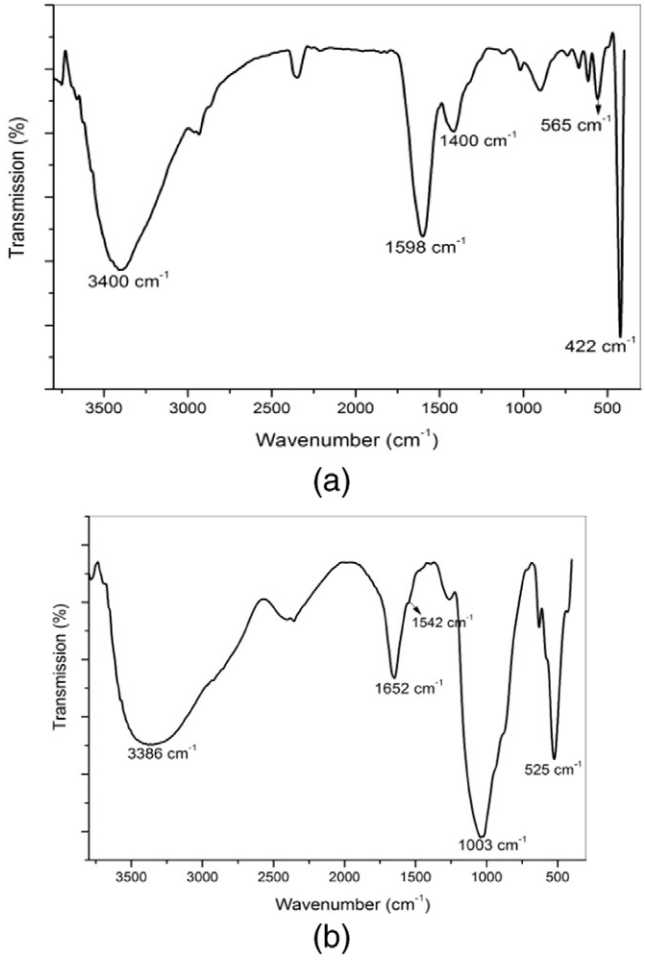

Fig. 4. FTIR spectra of (a) flower-like ZnO nanostructures and (b) urease immobilized on flower-like ZnO nanostructures prepared in a 0.01 M growth solution.

electrostatic interactions. The absorption band observed at 1542 cm^{-1} corresponds to C–N stretching and N–H bending modes of amide I bands and the absorption band at 1652 cm^{-1} corresponds to N–H stretching in amide II. The band at 1003 cm^{-1} can be assigned to C–O stretching. It may be seen that after immobilization of urease onto the ZnONF based matrix a strong absorption band at wavenumber corresponding to 525 cm^{-1} can be seen which may be occurring due to electrostatic interaction of Zn–O with the urease.

3.3. Electrochemical studies

A key point in the fabrication of the bioelectrode is that the immobilization platform should provide a large surface area for high enzyme loading and from the SEM images (Fig. 1(a)) it can be seen that ZnONF samples grown in a 0.005 M concentrated solution show only the formation of ZnO nanorods, while those grown in 0.01 and 0.02 M solutions (Fig. 1(b) and (c)) show the formation of flower-like morphologies in addition to the ZnO nanorods which would provide much higher surface area for enzyme immobilization. Hence, flower-like ZnO nanostructures based electrodes have been employed for the biosensor fabrication. Fig. 5 shows the cyclic voltammograms (CV) obtained for the Pt/Ti/Si electrode (curve (i)) in the potential window of −0.4 V to +0.8 V at the scan rate of 100 mV/s recorded in 50 mM PBS solution containing 5 mM $[Fe(CN)_6]^{3-/4-}$ as the redox species. The cyclic voltammograms for the two flower-like ZnO nanostructure based electrodes prepared in 0.01 M and 0.02 M growth solutions were also recorded and it was observed that both the electrodes exhibited similar CV responses (RSD ~ 1%). Hence, the CV response of one of the ZnONF/Pt/Ti/Si electrodes (0.01 M) is shown in curve (ii), Fig. 5. The cyclic voltammogram shows well defined oxidation and reduction peaks in the presence of $[Fe(CN)_6]^{3-/4-}$ mediator which provides an electron communication path at a lower potential. It can be seen from Fig. 5 that the peak oxidation current for the ZnONF/Pt/Ti/Si electrode (0.25 mA) is less as compared to that obtained for Pt/Ti/Si electrode (0.51 mA) due to relatively reduced electron mobility at the surface of electrode having ZnONF matrix thereby lowering the electron transfer. The oxidation and reduction peaks for the Pt/Ti/Si electrodes were found to be located at 0.27 V and 0.07 V respectively while those for the ZnONF/Pt/Ti/Si were located at 0.28 V and 0.08 V respectively showing almost a similar peak to peak separation voltage (~0.20 V). The obtained results show that the incorporation of flower-like ZnO nanostructures doesn't affect much the electron transfer kinetics. Thereafter, CVs were obtained after immobilization of urease on the surface of both the nanostructured electrodes grown in 0.01 M concentration (i.e. Urs/ZnONF1/Pt/Ti/Si) and 0.02 M concentration (i.e. Urs/ZnONF2/Pt/Ti/Si). The magnitude of the peak oxidation current was found to decrease further to 0.14 mA for Urs/ZnONF1/Pt/Ti/Si bioelectrode (Fig. 5, curve (iii)) and 0.10 mA for Urs/ZnONF2/Pt/Ti/Si bioelectrode (Fig. 5, curve (iv)) along with an increase in peak to peak separation potential of the redox peaks (~0.28 V) in comparison with that obtained for the ZnONF/Pt/Ti/Si electrode (~0.20 V). Such behavior is due to the insulating nature of the macromolecules of immobilized urease enzyme onto the nanostructured ZnO surface which obstructs the transfer of electrons between the electrode and the electrolyte. It is important to point out that when no mediator was present in the PBS solution, no oxidation–reduction peaks were observed for both the Urs/ZnONF1/Pt/Ti/Si and Urs/ZnONF2/Pt/Ti/Si bioelectrodes in the potential window of −0.4 V to +0.8 V indicating that the prepared bioelectrode does not have its own redox properties.

Inset (a) in Fig. 5 shows the electrochemical impedance spectra (EIS), of Pt/Ti/Si electrode (curve (i)), ZnONF/Pt/Ti/Si electrode (curve (ii)), and Urs/ZnONF1/Pt/Ti/Si bioelectrode (curve (iii)) recorded in a phosphate buffer saline (PBS, 50 mM, pH, 7.0, 0.9% NaCl) solution containing 5 mM $[Fe(CN)_6]^{3-/4-}$. The experimentally obtained impedance spectra have been modeled using the equivalent electrical circuit i.e. Randles circuit (inset (a), Fig. 5) [31] where the electrode–solution

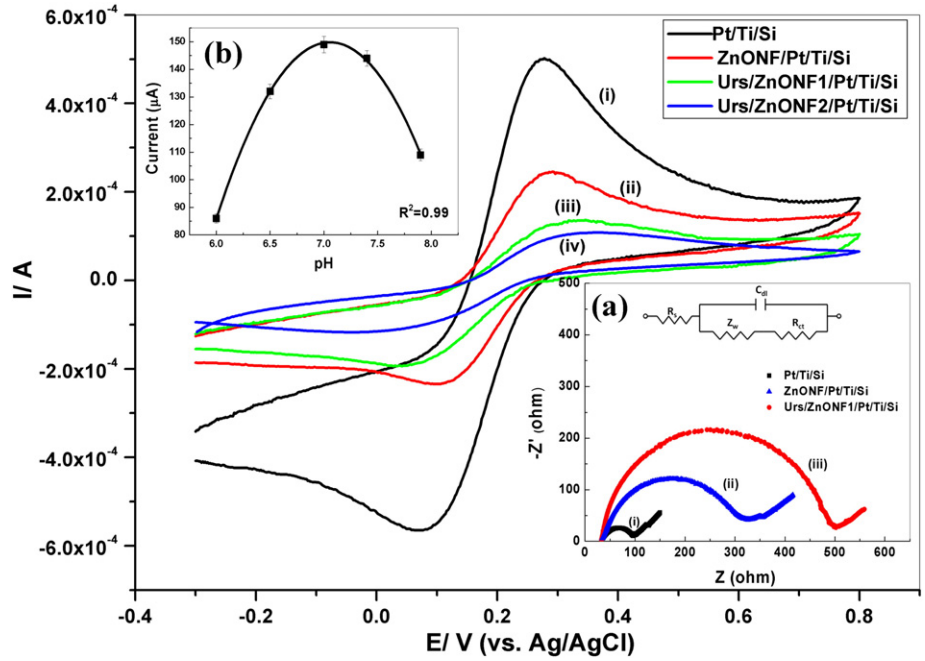

Fig. 5. Cyclic voltammograms of (i) Pt/Ti/Si, (ii) ZnONF/Pt/Ti/Si electrode, (iii) Urs/ZnONF1/Pt/Ti/Si and (iv) Urs/ZnONF2/Pt/Ti/Si bioelectrode recorded in PBS solution (PBS, 50 mM, pH 7.0, 0.9% NaCl) containing 5 mM $[Fe(CN)_6]^{3-/4-}$ as a redox mediator. Inset (a) shows EIS spectra of (i) Pt/Ti/Si electrode, (ii) ZnONF/Ti/Si electrode, (iii) Urs/ZnONF1/Pt/Ti/Si bioelectrode and inset (b) shows the effect on the current response of Urs/ZnONF1/Pt/Ti/Si bioelectrode for varying pH of 50 mM PBS solution containing 5 mM $[Fe(CN)_6]^{3-/4-}$ as a mediator.

interface is considered as a parallel combination of an interfacial resistor (R_{CT}) and double layer capacitor (C_{dl}) and the solution resistance is represented by a resistor (R_s). The contribution of Warburg impedance (Z_w), arising from the diffusion of the redox couple to and from the electrode, can be seen at low frequencies. The well-defined semicircles are observed in the EIS spectra of all prepared electrodes. The diameter of the semicircle is equal to electron-transfer resistance (R_{CT}) which controls the electron-transfer kinetics of the redox probe at the electrode interface. The value of R_{CT} obtained for Pt/Ti/Si is very low (~96 Ω) and increases to 0.32 kΩ when ZnONF are deposited on the surface of the Pt/Ti/Si substrate. The increase in the value of R_{CT} is attributed to the semiconducting nature of flower-like ZnO nanostructures which provides some barrier for the electron transfer between the electrode and mediated PBS solution, resulting in the delayed electron transfer kinetics on nanostructured ZnONF/Pt/Ti/Si electrode. After immobilization of urease onto ZnONF based electrode, the value of R_{CT}, further increases to 0.50 kΩ revealing that the immobilization of enzyme results in blocking the charge carriers due to the insulating nature of the enzyme. A similar increase in the R_{CT} value has also been observed for Urs/ZnONF2/Pt/Ti/Si bioelectrode.

Inset (b) in Fig. 5 shows the variation of the peak oxidation current for the Urs/ZnONF1/Pt/Ti/Si bioelectrode measured in the mediated buffer as a function of pH. It may be seen from inset (b) in Fig. 5 that the prepared bioelectrode shows maximum peak oxidation at a particular pH of ~7.0 of the buffer solution. This may be related to the fact that the activity of the biomolecules change with the pH of the surrounding ambient giving a maximum activity at a neutral pH of 7.0. Similarly, pH response was also obtained for Urs/ZnONF2/Pt/Ti/Si bioelectrode. Hence, all CV measurements in the present work have been carried out at pH 7.0 of the mediated PBS solution.

3.4. Electrochemical sensing response studies

The electrochemical sensing response of the Urs/ZnONF1/Pt/Ti/Si and Urs/ZnONF2/Pt/Ti/Si bioelectrodes as a function of the urea concentration is shown in Figs. 6 and 7 respectively. On addition of urea concentration into the buffer, the CV for Pt/Ti/Si and ZnONF/Pt/Ti/Si remains invariant (Fig. 5, curve (i) and (ii)) but Urs/ZnONF1/Pt/Ti/Si and Urs/ZnONF2/Pt/Ti/Si bioelectrodes show a change in the magnitude of redox peak currents. The variation of change in the CV peak currents with an increase in the urea concentration for Urs/ZnONF1/Pt/Ti/Si and Urs/ZnONF2/Pt/Ti/Si was studied. The well-defined CV curves are obtained for both the prepared bioelectrodes at all measured concentrations of urea (Figs. 6 and 7) showing a continuous increase in the magnitude of peak oxidation current with increase in urea concentration from 1.65–16.50 mM (i.e. 10–100 mg/dL) for Urs/ZnONF1/Pt/Ti/Si bioelectrode, while the Urs/ZnONF2/Pt/Ti/Si bioelectrode shows a comparatively lower urea detection range from 1.65–11.75 mM (i.e. 10–70 mg/dL) (Figs. 6 and 7). The chosen concentration range of urea in the present work is much wider than the physiological range of urea in human serum (2.5 to 7.5 mM). The variation in the magnitude of peak oxidation current as a function of urea concentration is shown in the insets (a) in Figs. 6 and 7. The results of triplicate sets indicated by error bars in the insets (a) in Figs. 6 and 7 reveal the reproducibility of measurements within ±5%, and show the higher reliability of prepared bio-electrode for urea detection. The sensitivities of the prepared bioelectrodes for urea have been calculated using the calibration curves (insets (a) in Figs. 6 and 7) and are found to be about 131.98 μA/mM/cm^2 and 67.62 μA/mM/cm^2 for Urs/ZnONF1/Pt/Ti/Si and Urs/ZnONF2/Pt/Ti/Si bioelectrodes respectively which is considerably much higher than the recently reported values for the urea biosensors based on the metal oxide matrices [31,43–46]. The obtained higher value of sensitivity of the biosensor is a consequence of high adsorption ability, effective enzyme loading and rapid electron communication characteristics of the flower-like ZnO nanostructure based matrix prepared in the present work. Furthermore, both the bioelectrodes exhibit a fast response towards urea, and attain 95% of the maximum steady state current in 4 s. The obtained results for sensing response are found to be much better compared with the corresponding reports available on nanostructured metal oxide based urea biosensor by other workers [31]. The sensing response measurements were repeated on different bioelectrode samples prepared separately in different batches under similar processing conditions and same results were obtained within experimental error indicating that the ZnONF based matrix gives reproducible results. A controlled experiment was also carried out in which plain Urs/Pt/Ti/Si electrode was prepared for urea detection. However

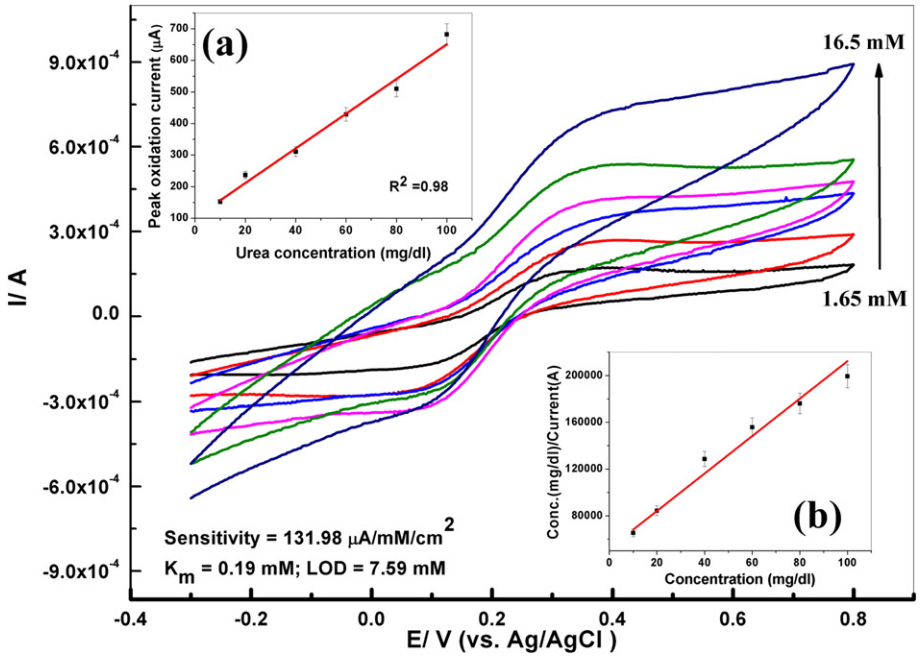

Fig. 6. Electrochemical sensing response of Urs/ZnONF1/Pt/Ti/Si bioelectrode taken in 50 mM PBS solution containing 5 mM $[Fe(CN)_6]^{3-/4-}$ mediator as a function of urea concentration (in mg/dL): (i) 10, (ii) 20, (iii) 40, (iv) 60, (v) 80, and (vi) 100. Inset (a) shows the variation of CV peak oxidation current as a function of urea concentration, and inset (b) shows the Hanes plot to determine the value of Michaelis–Menten constant (K_m).

no sensing response for the bioelectrode was obtained for the prepared different urea concentrations and no change in the magnitude of redox peak currents in the cyclic voltammogram was observed. On the other side the presence of nanostructure ZnO matrix is advantageous for the immobilization of urease on its surface using physical adsorption technique. The immobilized urease on the surface of ZnO matrix interacts with the analyte (urea) of varying urea concentrations thereby giving different values of peak oxidation current and hence, it can be concluded that the presence of ZnO nanostructure matrix is responsible for the detection of urea. The possible sensing mechanism of urea using the prepared bioelectrodes is shown in Scheme 2. The activity of urease is due to the SH group present on the active site of urease that can be oxidized by the chemical reaction with urea as given in Eq. (8).

$$CO(NH_2)_2 + H_2O \xrightarrow{\text{Urease}} 2NH_3 + CO_2. \quad (8)$$

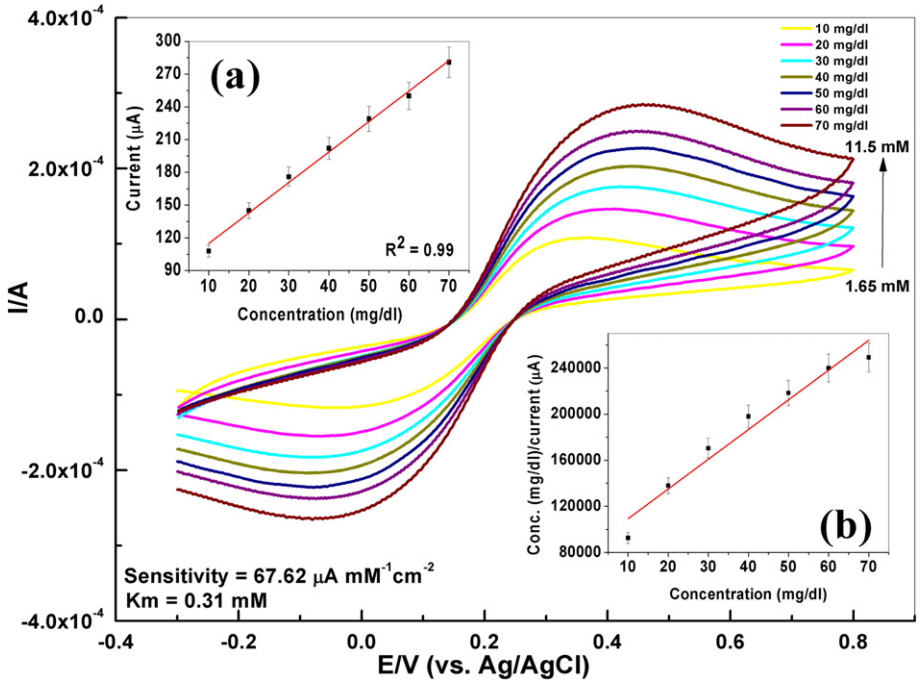

Fig. 7. Electrochemical sensing response of Urs/ZnONF2/Pt/Ti/Si bioelectrode taken in 50 mM PBS solution containing 5 mM $[Fe(CN)_6]^{3-/4-}$ mediator as a function of urea concentration (in mg/dL): (i) 10, (ii) 20, (iii) 30, (iv) 40, (v) 50, (vi) 60, and (vii) 70. Inset (a) shows the variation of CV peak oxidation current as a function of urea concentration, and inset (b) shows the Hanes plot to determine the value of Michaelis–Menten constant (K_m).

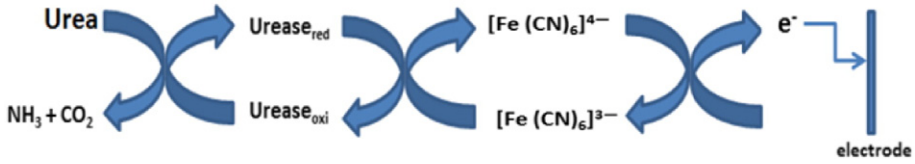

Scheme 2. Schematic of the electron exchange occurring at the surface of bioelectrode in the presence of redox species.

After oxidation, the S–S bond thus produced can be reduced back to the SH group by the electrode reactions, thus recovering the original enzyme activity [47]. Hence, as shown in Scheme 2, the reduced urease loses electrons which are subsequently captured by $[Fe(CN)_6]^{3-}$ ions present in the PBS buffer solution near the vicinity of the bioelectrode getting reduced to $[Fe(CN)_6]^{4-}$ ions. These in turn oxidize to $[Fe(CN)_6]^{3-}$ ions during forward CV scan at a potential of 0.44 V and thus transferring electrons to the bottom electrode i.e. platinum (Pt) in the present case via matrix utilizing the good electron communication feature of the nanostructured ZnO matrix. During the reverse CV scan the whole process is repeated in the reverse direction as shown in Scheme 2. Thus, as the urea concentration increases, biochemical reaction takes place resulting in the release of more number of electrons and hence, a corresponding increase in CV peak oxidation current is observed.

Insets (b) in Figs. 6 and 7 show Hanes plot (graph of [concentration/current] vs [concentration of urea]) which has been used to estimate the value of Michaelis–Menten constant (K_m) for the bioelectrodes [48]. The K_m value is found to be about 0.19 mM for Urs/ZnONF1/Pt/Ti/Si bioelectrode and 0.31 mM for Urs/ZnONF2/Pt/Ti/Si which is much lower compared with the earlier reported values for urea biosensors based on nanostructured metal oxide matrices [31,43–45]. The lower value of K_m indicates a high affinity of the immobilized urease enzyme towards its analyte (urea). The ZnO nanoflower matrix provides higher surface to volume ratio for the effective loading of the enzyme (Urs) having favorable conformational changes on the enzyme surface and resulting in a much lower value of K_m. Thus, on comparing the electrochemical response of both the bioelectrodes it can be clearly seen that the performance of Urs/ZnONF1/Pt/Ti/Si bioelectrode is much better as compared with the Urs/ZnONF2/Pt/Ti/Si bioelectrode in terms of detection range, sensitivity and K_m value. This may be attributed to the fact that the surface morphology of Urs/ZnONF1/Pt/Ti/Si bioelectrode supports favorable orientation of the biomolecules and induces such kind of conformational changes which lead to the activation of enzymatic redox centers of the biomolecules hence, leading to enhanced response. Thus, Urs/ZnONF1/Pt/Ti/Si bioelectrode has been utilized in the further studies.

Nanoparticles can also be utilized for the bioelectrode fabrication but they need to be functionalized in order to immobilize enzyme on its surface using chemical treatment. On the contrary, flower-like ZnO nanostructures do not demand the functionalization and urease was immobilized by simple physical adsorption technique, thus resulting in reliable nanostructured bioelectrode. The fabrication of urea biosensor based on ZnO nanoparticles (NPs) was reported by other workers where NPs were functionalized using chitosan [43]. There is another report by Kaushik et al. where iron oxide (Fe_3O_4) nanoparticles and chitosan have been used for urea detection [44]. The reported results on urea biosensing are found to be comparatively inferior to those obtained in the present work (Table 2). The enhanced response characteristics are due to the favorable microenvironment provided by the synthesized flower-like ZnO nanostructures for conformal immobilization of the urease besides effective loading of enzyme and good electron communication feature. The observed results clearly indicate the importance of ZnO flower-like nanostructures used in the present work over the nanoparticles for urea biosensing applications. Gold nanoparticles (AuNPs) can also increase the electroconductivity of the matrix, however the cost and functionalization issues are critical. Further effective loading and conformal immobilization of the urease are advantageous for the flower-like ZnO nanostructure matrix. Parashar et al. have demonstrated the urea sensing using gold nanoparticles [50]. However, the biosensing results obtained using flower-like ZnO nanostructure matrix are found to be much superior to those reported using AuNPs [50].

3.5. Effect of scan rate

The CV studies were conducted on the prepared Urs/ZnONF/Pt/Ti/Si bioelectrode as a function of scan rate from 160 to 250 mV/s (Fig. 8) to determine the concentration of the ionic species available on its surface. A continuous shifting of the oxidation peak towards higher potential and the reduction peak towards lower potential are observed with an increase in scan rate indicating that the oxidation–reduction process for the prepared Urs/ZnONF/Pt/Ti/Si bioelectrode is a quasi-reversible process [48]. Inset (a) in Fig. (8) shows the linear variation in redox peak currents (peak oxidation, I_{po} and peak reduction, I_{pr}) as a function of square root of scan rate. The linear regression equations fitted to the variation of both peak oxidation (I_{po}) and peak reduction (I_{pr}) currents (inset (a) in Fig. 8) are given as:

$$I_{po} = 53.88\nu^{1/2} - 384.15 \quad \text{with } R^2 = 0.999 \tag{4}$$

$$I_{pr} = -40.88\nu^{1/2} + 263.76 \quad \text{with } R^2 = 0.999 \tag{5}$$

where, R^2 is regression coefficient. Value of R^2 close to 1.0 indicates that both the oxidation (I_{po}) and reduction (I_{pr}) peak currents increase linearly with the square root of scan rate ($\nu^{1/2}$), suggesting that the reaction on the prepared electrode is a diffusion assisted electron-transfer process [49]. The plot of oxidation peak potential (E_{po}) with logarithm of scan rate (ν) is also found to be linear and is shown in inset (b) in

Table 2
A comparative study of metal oxide based urea biosensors.

Matrix	Detection range (mM)	K_m (mM)	Sensitivity ($\mu A\ mM^{-1}\ cm^{-2}$)	Response time (s)	Shelf life (weeks)	Ref.
TiO_2–ZrO_2 composite	0.8–16.6	–	2.74	10	6	[19]
ZnO thin film	0.8–13.3	1.01	8.70	–	–	[31]
ZnO nanorods	1–20	9.09	0.40	3	–	[32]
ZnO–chitosan composite	0.8–16.6	0.82	0.13	10	12	[43]
Chitosan–Fe_3O_4 composite	0.8–16.6	0.56	12.50	10	8	[44]
ZrO_2 thin film	0.8–16.6	0.50	0.07	10	16	[45]
Flower-like ZnO nanostructures	1.65–16.6	0.19	131.98	4	12	Present work

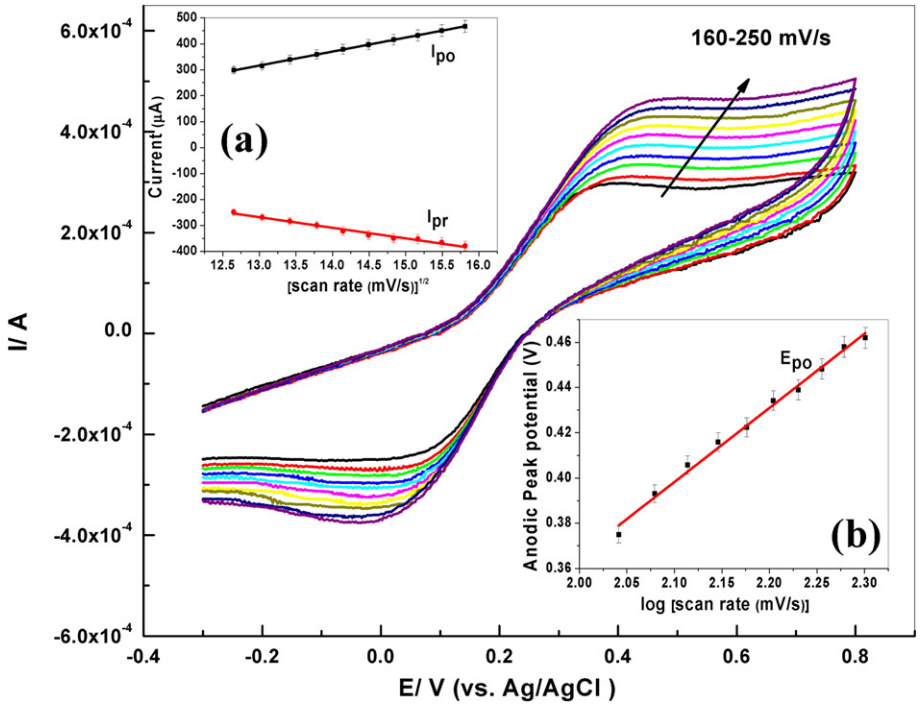

Fig. 8. CV curves for the Urs/ZnONF1/PT/Ti/Si bioelectrode taken at different scan rates in 50 mM PBS solution containing 5 mM $[Fe(CN)_6]^{3-/4-}$ as a mediator. Inset (a) shows the variation of peak current (oxidation; I_{po} and reduction; I_{pr}) as a linear function of the square root of scanning rate and inset (b) shows the variation in anodic peak potential (E_{po}) as a function of logarithm of scan rate.

Fig. 8. The concentration (Γ) of the ionic species per unit surface area available on Urs/ZnONF/Pt/Ti/Si bioelectrode is estimated using the Brown–Anson model [51] based on the following equation:

$$I_{po} = \frac{n^2 F^2 \Gamma A \nu}{4RT} \quad (6)$$

where Γ is the estimated value of surface coverage in mol cm^{-2}, n is the number of electrons transferred, F is the Faraday constant (96,485 C mol^{-1}), A is the surface area (0.25 cm^{-2}) of electrode, R is the gas constant (8.314 J mol^{-1} K^{-1}), and T is the temperature (298 K). The value of I_{po}/ν can be obtained from the slope of the plot between I_{po} (oxidation peak current) vs. ν (scan rate in mV/s). The estimated value of Γ is found to be about 3.16×10^{-7} mol cm^{-2} which shows an effective loading or immobilization of urease onto the surface of flower-like ZnO nanostructure based matrix. The value of surface concentration of the ionic species obtained in the present case is found to be higher as compared with the corresponding reported values for enzymatic urea biosensors by other workers and is due to a significant increase in the surface area of the nanostructured ZnO [43]. Since, the surface area provided by the matrix is related to the effective loading of the enzyme on its surface. In order to confirm the effective loading of the enzyme and hence surface area provided by the flower-like ZnO nanostructures (ZnONF1) prepared using 0.01 M precursor is higher as compared with that of ZnO nanorods (ZnONF3) and nanoflowers (ZnONF2) prepared using 0.005 M and 0.02 M precursors respectively. The scan rate study for the remaining two bioelectrodes i.e. for Urs/ZnONF2/Pt/Si and Urs/ZnONF3/Pt/Si was also performed and the results are shown in supplementary Figs. 1 and 2 in the revised manuscript. The surface concentrations of the ionic species present on the surface of the Urs/ZnONF2/Pt/Ti/Si and Urs/ZnONF3/Pt/Ti/Si bioelectrodes as calculated are 7.23×10^{-10} mol cm^{-2} and 4.85×10^{-10} mol cm^{-2} respectively. The observed values are found to be significantly lower by about three orders of magnitude in comparison with that obtained for Urs/ZnONF1/Pt/Ti/Si electrode (3.16×10^{-7} mol cm^{-2}) based on flower-like ZnO nanostructure (prepared using a 0.01 M precursor). This clearly shows that there is higher loading of urease molecules over the surface of ZnO flower-like nanostructures (0.01 M precursor) compared with other prepared matrices and is related to a larger surface area provided by the flower-like ZnO nanostructure matrix.

The obtained results clearly indicate that the prepared ZnONF based matrix provides an efficient platform for the immobilization of urease enzyme thus giving a higher concentration of ionic species on its surface.

The diffusion coefficient value (D) of Urs/ZnONF/Pt/Ti/Si electrode has been estimated using Randels–Sevcik equation [31] given as:

$$I_p = \left(2.69 \times 10^5\right) n^{3/2} A\, D^{1/2} \Gamma \nu^{1/2} \quad (7)$$

where, I_p is the peak current, n is the number of electrons transferred ($n = 1$) and D is the diffusion coefficient. The value of the slope obtained from the plot of I_p versus $\nu^{1/2}$ is used in Eq. (7) to estimate the value of D. The estimated value of D is found to be about 5.63×10^{-3} cm^2 s^{-1} which is much higher than the corresponding value reported by other workers for nanostructured ZnO matrix [31].

3.6. Interference and shelf-life studies

The selectivity of Urs/ZnONF1/Pt/Ti/Si bioelectrode is determined by measuring the peak oxidation current in CV obtained on addition of normal concentration of other interferents in the human blood/serum such as glucose (glu) (5.6 mM), cholesterol (cho) (5 mM), uric acid (UA) (0.1 mM), ascorbic acid (AA) (0.05 mM) and lactic acid (AA) (5 mM) along with the normal concentration of urea (1.6 mM) and the obtained value of CV peak oxidation current is plotted in the form of the bar graph (Fig. 10). It may be observed that the maximum interference has been obtained for uric acid (UA) which is found to be only 4.1%. The interference study was also carried out in the absence of urea. The peak oxidation current for Urs/ZnONF1/Pt/Ti/Si bioelectrode shows an insignificant increase from 0.13 mA to 0.14 mA on addition of 0.1 mM UA in the buffer solution in the absence of urea. The observed value of

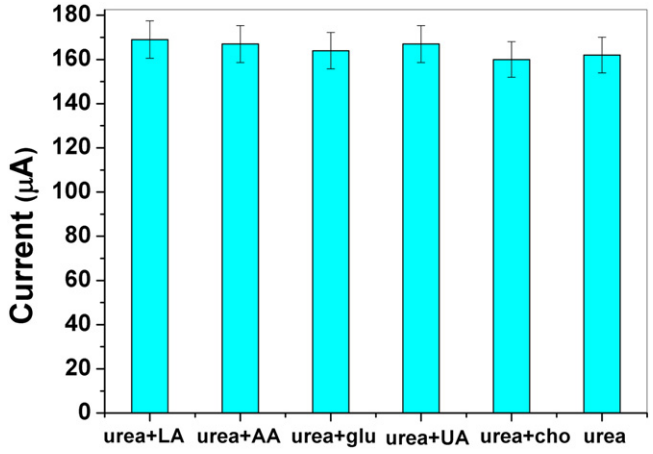

Fig. 9. Photometric assay of Urs/ZnONF1/Pt/Ti/Si bioelectrode as a function of urea concentration.

oxidation peak current is close to the baseline value (corresponding to the 0 mM urea concentration). Hence, the prepared bioelectrode (Urs/ZnONF1/Pt/Ti/Si) is highly selective towards specific detection of urea. The detection limit of Urs/ZnONF1/Pt/Ti/Si bioelectrode is estimated using 3(S.D.)/*m* criteria, where *m* is slope of the calibration graph and S.D.is standard deviation of the blank signal and is found to be a very low detection limit of 5 mg/dL (0.83 mM) as compared with the available reported value in literature [31]. The shelf life study (as shown in Fig. 10) of the bioelectrode was performed by measuring the peak oxidation current after regular interval of time. It is found that the bioelectrode retains more than 90% of its activity even after 12 weeks i.e. about 3 months of storage at 4 °C which is higher as compared with the available reported value [19,14]. This may be attributed to the preparation of highly stable and biocompatible matrix of flower-like ZnO nanostructures, having favorable surface for efficient loading of the urease enzyme used in the present study.

3.7. Photometric enzyme assay

A photometric response study was performed to calculate the apparent enzyme activity of the bioelectrode (Urs/ZnONF1/Pt/Ti/Si) using a UV–visible spectrophotometer. For photometric measurements, Urs/ZnONF1/Pt/Ti/Si bioelectrode was dipped in a 3 mL PBS solution (50 mM, pH7.0), containing 10 μL of Nessler's solution and 100 μL of urea solution with varying concentrations. The Urs/ZnONF1/Pt/Ti/Si bioelectrode was incubated in the prepared solution for 2 min and a colored complex was formed i.e., $NH_2Hg_2I_3$, between the Nessler's reagent and ammonia produced by the enzymatic hydrolysis of urea. The absorbance of the solution was measured at λ_{max} equal to 385 nm, to monitor the Urs enzyme kinetics for different concentrations of urea [52]. The difference between the initial and final absorbance values at $\lambda =$ 385 nm obtained before and after incubating Urs/ZnONF1/Pt/Ti/Si bioelectrode in the solution was plotted as a function of urea concentration (Fig. 11). It may be seen from Fig. 9 that the absorbance initially increases linearly with an increase in urea concentration up to 40 mg/dL and thereafter shows the saturation tendency indicating that the maximum number of biomolecules present on the bioelectrode surface has participated in the chemical reaction. The apparent enzyme activity (a^{enz}_{app}) of the bioelectrode was calculated using equation:

$$a^{enz}_{app} = \frac{A'V}{\varepsilon t A} \tag{9}$$

where, A′ is the absorbance obtained for the solution having a urea concentration that shows saturating absorbance (80 mg/dL in present work), V is the total volume of the solution (3.17 cm^3), ε is the millimolar extinction coefficient of the Nesseler's reagent, t is the reaction time (2 min) and A is the surface area of the bioelctrode (0.25 cm^2). The estimated value of apparent enzyme activity was about 1.37×10^{-1} Units/cm^2. The value of apparent enzyme activity obtained for the prepared bioelectrode in the present work is found to be much higher compared with the corresponding values obtained for other ZnO based biosensors [53] indicating that higher units of urease are actively working per unit surface area of electrode based on flower-like ZnO nanostructures.

A comparison table (Table 2) has been included for comparing the presently fabricated ZnO nanostructured biosensor with other metal oxide based urea biosensors reported in literature for highlighting the importance of the present work. The Urs/ZnONF/Ti/Pt/Si bioelectrode has also been employed for the analysis of the real samples (human serum) and the urea concentration values of different human serum samples were determined. The obtained results were found to be in close agreement with the corresponding values as obtained from the clinical lab using spectrophotometric techniques with a maximum RSD of 1.2% which shows very good accuracy in measurement of urea concentration in real samples using Urs/ZnONF1/Pt/Ti/Si bioelectrode. After spiking the real samples with 0.3 mM urea concentration the recovery studies were performed and almost 100% recovery was observed for all the real samples showing satisfactory recovery.

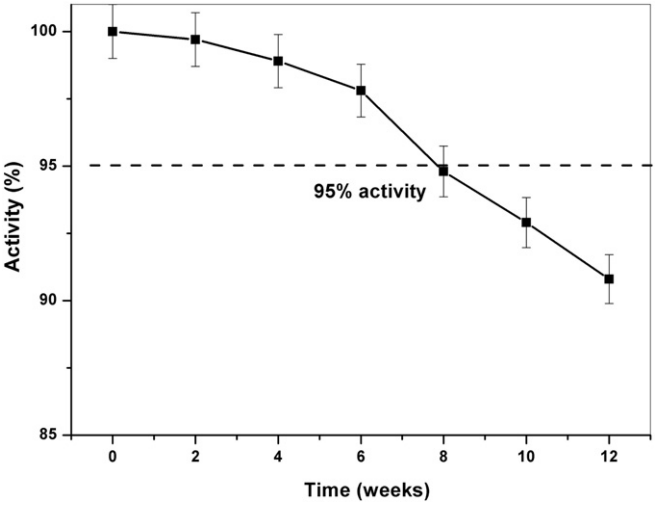

Fig. 10. The effect of interferents on Urs/ZnONF1/Pt/Ti/ bioelectrode.

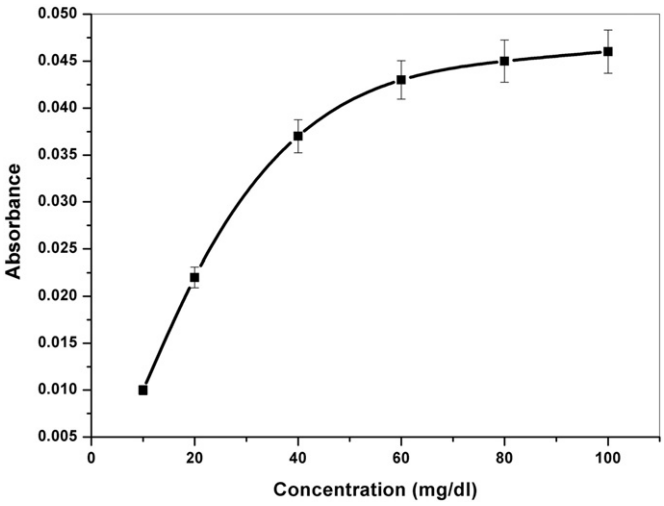

Fig. 11. The shelf life study of the Urs/ZnONF1/Pt/Ti/Si bioelectrode.

4. Conclusions

Flower-like ZnO nanostructure based matrix has been synthesized by hydrothermal method and has been exploited efficiently for detection of urea. Nanostructured zinc oxide matrix has higher surface to volume ratio and provides favorable platform for efficient loading of urease enzyme via physical adsorption. The bioelectrode (Urs/ZnONF1/Pt/Ti/Si) shows a fast response time of 4 s over a wide range of concentration of urea from 1.65 mM to 16.50 mM with relatively low detection limit of 0.90 mM. The high sensitivity of ~132 μA/mM/cm^2, high apparent enzyme activity of 1.37×10^{-1} Units/cm^2 and low K_m value of 0.19 mM highlight the importance of synthesized ZnONF matrix which provides a suitable microenvironment for the immobilized urease preserving its biological activity along with favorable conformational changes on its surface. The high selectivity as well as stability of the bioelectrode (Urs/ZnONF1/Pt/Ti/Si) may pave the way towards realization of an efficient biosensor for a reliable detection of urea.

Acknowledgments

The authors are thankful to Department of Science and Technology (DST), Govt. of India for the financial support to carry out this work. One of the authors (MT) is thankful to UGC for the research fellowship.

Appendix A. Supplementary data

Supplementary data to this article can be found online at http://dx.doi.org/10.1016/j.msec.2015.06.052.

References

[1] H. Beitollahi, I. Sheikhshoaie, Int. J. Electrochem. Sci. 9 (2014) 2955–2965.
[2] H. Beitollahi, I. Sheikhshoaie, Anal. Methods 3 (2011) 1810–1814.
[3] E. Molaakbari, A. Mostafavi, H. Beitollahi, R. Alizadeh, Analyst 139 (2014) 4356–4364.
[4] H. Beitollahi, A. Mohadesi, S. Mohammadi, A. Akbari, Electrochim. Acta 68 (2012) 220–226.
[5] H. Beitollahi, I. Sheikhshoaie, Electrochim. Acta 56 (2011) 10259–10263.
[6] H. Beitollahi, M. Mostafavi, Electroanal. 26 (2014) 1090–1098.
[7] H. Beitollahi, I. Sheikhshoaie, Int. J. Electrochem. Sci. 7 (2012) 7684–7698.
[8] H. Beitollahi, I. Sheikhshoaie, J. Electroanal. Chem. 661 (2011) 336–342.
[9] H.M. Moghaddam, H. Beitollahi, Int. J. Electrochem. Sci. 6 (2011) 6503–6513.
[10] G. Dhawan, G. Sumana, B.D. Malhotra, Biochem. Eng. J. 44 (2009) 42–52.
[11] C.J. Pattson, S.R. Crouch, Anal. Chem. 49 (1977) 464–469.
[12] F. Roch-Ramel, Anal. Biochem. 21 (1967) 372–381.
[13] K. Chen, D. Liu, L. Nie, S. Yao, Talanta 41 (1994) 2195–2200.
[14] W.O. Ho, S. Krause, C.J. McNeil, J.A. Pritchard, R.D. Armstrong, D. Athey, K. Rawson, Anal. Chem. 71 (1999) 1940–1946.
[15] D.G. Pijanowska, W. Torbicz, Sensors Actuators B 44 (1997) 370–376.
[16] E. Prats-Alfonso, L. Abad, N. Casan˜-Pastor, J. Gonzalo-Ruiz, E. Baldrich, Biosens. Bioelectron. 39 (2013) 163–169.
[17] S.G. Ansari, R. Wahab, Z.A. Ansari, Y. Kim, G. Khang, A. Al-Hajry, H. Shin, Sensors Actuators B 137 (2009) 566–573.
[18] R.S. De, C.R. Raj, J. Phys. Chem. C 114 (2010) 21427–21433.
[19] S. Srivastava, A. Ali, P.R. Solanki, P.M. Chavhan, M.K. Pandey, A. Mulchandani, A. Srivastava, B.D. Malhotra, RSC Adv. 3 (2013) 228–235.
[20] E.M. Çevik, A. Şenel Baykal, Curr. Appl. Phys. 13 (2013) 280–286.
[21] M. Zhao, J. Huang, Y. Zhou, Q. Chen, X. Pan, H. He, Z. Ye, Biosens. Bioelectron. 43 (2013) 226–230.
[22] M. Baghayeria, E.N. Zare, M. Namadchian, Sensors Actuators B 188 (2013) 227–234.
[23] M. Baghayeri, E.N. Zare, M.M. Lakouraj, Biosens. Bioelectron. 55 (2014) 259–265.
[24] M. Baghayeri, E.N. Zare, R. Hasanzade, Mat. Sci. Eng. C 39 (2014) 213–220.
[25] M. Baghayeria, E.N. Zare, M.M. Lakouraj, Sensors Actuators B 202 (2014) 1200–1208.
[26] M. Baghayeri, E.N. Zare, M.M. Lakouraj, Microchim. Acta 182 (2015) 771–779.
[27] M. Baghayeri, H. Veisi, B. Maleki, H.K. Maleh, H. Beitollahi, RSC Adv. 4 (2014) 49595.
[28] P.R. Solanki, A. Kaushik, V.V. Agrawal, B.D. Malhotra, NPG Asia Mater. 3 (2011) 17–24.
[29] S. Saha, V. Gupta, K. Sreenivas, H.H. Tan, C. Jagadish, Appl. Phys. Lett. 97 (2010) 133704.
[30] T. Kong, Y. Chen, Y. Ye, K. Zhang, Z. Wang, X. Wang, Sensors Actuators B 138 (2009) 344–350.
[31] A. Ali, A.A. Ansari, A. Kaushik, P.R. Solanki, A. Barik, M.K. Pandey, B.D. Malhotra, Mater. Lett. 63 (2009) 2473–2475.
[32] N. Palomera, M. Balaguera, S.K. Arya, S. Hernández, M.S. Tomar, J.E. Ramírez-Vick, S.P. Singh, J. Nanosci. Nanotechnol. 11 (2011) 6683.
[33] J.S. Huang, C.F. Lin, IEEE Sensors J. 978 (2008) 315–318.
[34] Z. Liu, J. Ya, E. Lei, J. Solid State Electrochem. 14 (2010) 957–963.
[35] S. Baruah, J. Dutta, Sci. Technol. Adv. Mater. 10 (2009) 013001.
[36] S.F. Lee, L.Y. Lee, Y.P. Chang, J. Sci. Eng. Technol. 5 (2009) 13–20.
[37] R. Wahab, S.G. Ansari, Y.S. Kim, H.K. Seo, G.S. Kim, G. Khang, H.S. Shin, MRS Bull. 42 (2007) 1640–1648.
[38] Z.L. Wang, X.Y. Kong, Y. Ding, P.X. Gao, W.L. Hughes, R.S. Yang, Y. Zhang, Adv. Funct. Mater. 14 (2004) 943–956.
[39] P.X. Gao, Z.L. Wang, J. Phys. Chem. B 108 (2004) 7534.
[40] A. Mahmood, N. Ahmed, Q. Raza, T.M. Khan, M. Mehmood, M.M. Hassan, N. Mahmood, Phys. Scr. 82 (2010) 065801.
[41] N. Mehan, V. Gupta, K. Sreenivas, A. Mansingh, J. Appl. Phys. 96 (2004) 3134–3139.
[42] R. Gopikrishnan, K. Zhang, P. Ravichandran, S. Baluchamy, V. Ramesh, S. Biradar, P. Ramesh, J. Pradhan, J.C. Hall, A.K. Pradhan, G.T. Ramesh, Nano-Micro Lett. 2 (2010) 31–36.
[43] P.R. Solanki, A. Kaushik, A.A. Ansari, G. Sumana, B.D. Malhotra, Appl. Phys. Lett. 93 (2008) 163903.
[44] A. Kaushik, P.R. Solanki, A.A. Ansari, G. Sumana, S. Ahmad, B.D. Malhotra, Sensors Actuators B 138 (2009) 572–580.
[45] G. Sumana, M. Das, S. Srivastava, B.D. Malhotra, Thin Solid Films 519 (2010) 1187–1191.
[46] M. Tyagi, M. Tomar, V. Gupta, Biosen. Bioelectron. 41 (2013) 110–115.
[47] S. Uchiyama, M. Kobayashi, Y. Hasebe, Electroanal 14 (2002) 1644–1647.
[48] K. Jindal, M. Tomar, V. Gupta, Biosens. Bioelectron. 38 (2012) 11–18.
[49] K. Arora, M. Tomar, V. Gupta, Biosens. Bioelectron. 30 (2011) 333–336.
[50] U.K. Parashar, N.R. Nirala, C. Upadhyay, P.S. Saxenan, A. Srivastava, Appl. Biochem. Biotechnol. 176 (2015) 480–492.
[51] M. Tyagi, M. Tomar, V. Gupta, Anal. Chim. Acta 726 (2012) 93–101.
[52] A. Tiwari, S. Aryal, S. Pilla, S. Gong, Talanta 78 (2009) 1401–1407.
[53] S. Saha, V. Gupta, J. Appl. Phys. 110 (2011) 064904.